Received: 3 February 2021 | Revised: 14 April 2021 | Accepted: 14 April 2021

DOI: 10.1111/cas.14924

ORIGINAL ARTICLE

Cancer Science WILEY

PP1 regulatory subunit NIPP1 regulates transcription of E2F1 target genes following DNA damage

Shunsuke Hanaki[1] | Makoto Habara[1] | Takahiro Masaki[1] | Keisuke Maeda[1] | Yuki Sato[1] | Makoto Nakanishi[2] | Midori Shimada[1]

[1]Department of Biochemistry, Joint Faculty of Veterinary Science, Yamaguchi University, Yamaguchi, Japan

[2]Division of Cancer Biology, Institute of Medical Science, The University of Tokyo, Tokyo, Japan

Correspondence
Midori Shimada, Department of Biochemistry, Joint Faculty of Veterinary Science, Yamaguchi University, 1677-1 Yoshida, Yamaguchi, 753-8511, Japan.
Email: shimada@yamaguchi-u.ac.jp

Funding information
Japanese Society for the Promotion of Science, Grant/Award Number: 18H02681; MSD Life Science Foundation, Public Interest Incorporated Foundation

Abstract

DNA damage induces transcriptional repression of E2F1 target genes and a reduction in histone H3-Thr^{11} phosphorylation (H3-pThr^{11}) at E2F1 target gene promoters. Dephosphorylation of H3-pThr11 is partly mediated by Chk1 kinase and protein phosphatase 1γ (PP1γ) phosphatase. Here, we isolated NIPP1 as a regulator of PP1γ-mediated H3-pThr^{11} by surveying nearly 200 PP1 interactor proteins. We found that NIPP1 inhibits PP1γ-mediated dephosphorylation of H3-pThr^{11} both in vivo and in vitro. By generating NIPP1-depleted cells, we showed that NIPP1 is required for cell proliferation and the expression of E2F1 target genes. Upon DNA damage, activated protein kinase A (PKA) phosphorylated the NIPP1-Ser^{199} residue, adjacent to the PP1 binding motif (RVxF), and triggered the dissociation of NIPP1 from PP1γ, leading to the activation of PP1γ. Furthermore, the inhibition of PKA activity led to the activation of E2F target genes. Statistical analysis confirmed that the expression of NIPP1 was positively correlated with E2F target genes. Taken together, these findings demonstrate that the PP1 regulatory subunit NIPP1 modulates E2F1 target genes by linking PKA and PP1γ during DNA damage.

KEYWORDS
DNA damage, E2F1, histone phosphorylation, protein phosphatase, transcription

1 | INTRODUCTION

The post-translational modification of histones is a central mechanism for the regulation of gene expression. In a previous study, we found that the phosphorylation of Thr at position 11 of histone H3 (H3-Thr^{11}) at the promoter regions of E2F1-targeted genes, such as cyclin-dependent kinases (Cdks).[1] H3-Thr^{11} phosphorylation is mediated by binding of checkpoint kinase 1 (Chk1) to chromatin, followed by the recruitment of histone acetyltransferase GCN5 to H3-Thr^{11}. GCN5, in turn, elicits the acetylation of lysine at position 9 of histone H3 (H3-Lys^{9}) at the promoters of cell cycle regulatory genes, leading to the upregulation of transcription. Upregulated Cdks phosphorylate PP1γ on Thr at position 311 (PP1γ-Thr^{311}), which inhibits PP1γ activity to maintain the phosphorylation of H3-Thr^{11}.[2]

Protein kinases and phosphatases mediate optimal cellular responses to DNA damage to promote survival and suppress genetic instability.[3] DNA damage activates ataxia telangiectasia and Rad3-related protein (ATR) kinase, which phosphorylates Chk1, causing Chk1 to dissociate from chromatin.[1] We also previously showed that dissociation of Chk1 induces the rapid dephosphorylation of H3-Thr^{11}, reciprocally causing a reduction in acetylated H3-Lys^{9} and suppressing Cdk activity. Inactivation of Cdks has also been shown

to enhance PP1γ activity upon DNA damage, which further consolidates the dephosphorylation status of H3-Thr^{11} and restrains the cell cycle.

In general, PP1 activity is regulated by phosphorylation mediated by Cdk1, and by binding to a regulatory subunit.[4] However, the mechanism by which PP1 activity toward H3-pThr^{11} increases as a result of DNA damage via the interaction of PP1 with its regulatory subunit remains poorly understood. PP1 activity is modulated by the association of PP1 interacting proteins (PIPs), which regulate the specificity and diversity of PP1 function.[5] Therefore, in the present study, the regulatory factors involved in PP1-mediated histone H3 dephosphorylation at Thr^{11} were explored by conducting a Gene Ontology (GO) analysis of the PP1 interactome database. As a result, NIPP1 (nuclear inhibitor of protein phosphatase 1) was identified as a potential candidate.

NIPP1 is involved in key cellular processes, such as splicing and transcription, and exerts its functions via its interactions with PP1.[6,7] Indeed, NIPP1 was initially discovered as a potent inhibitor and a major nuclear interactor of PP1.[8,9] Consistent with this notion, NIPP1 acts as a physiological PP1 inhibitor for certain substrates of PP1. However, NIPP1 can also function as an activator toward other substrates.[10] Furthermore, the interaction between NIPP1 and PP1 can be regulated by phosphorylation. For example, NIPP1-PP1 association is decreased upon NIPP1 phosphorylation, mediated by protein kinase A (PKA) (Ser^{199}), casein kinase 2 (CK2) (Ser^{204}), or protein tyrosine kinases of the Src family (Tyr^{335}).[11-14]

In the present study, NIPP1 was shown to be a regulatory subunit of PP1γ for H3-pThr^{11} dephosphorylation. NIPP1 inhibits PP1γ and, in this way, promotes H3-Thr^{11} phosphorylation, which eventually results in the activation of E2F target genes and the promotion of the cell cycle. Upon DNA damage, NIPP1 is phosphorylated on Ser at position 199 (NIPP1-Ser^{199}) by PKA, leading to the dissociation of NIPP1 from PP1γ. Activated PP1γ dephosphorylates H3-pThr^{11} in collaboration with Chk1 released from E2F1 target genes. Ultimately, this results in the transcriptional repression of genes, such as *CDK1* and *CCNB1*, involved in the cell cycle,. Collectively, the findings presented in this study suggest a novel link between PKA, PP1γ, and NIPP1 during the cellular response to DNA damage.

2 | MATERIALS AND METHODS

2.1 | Cell culture, reagents, and UV irradiation

HCT116 cells were cultured in McCoy's 5A medium (16600-082; Gibco) containing 10% FBS and antibiotics (15240062; Thermo Fisher Scientific). HEK293T cells were cultured in DMEM (044-29765; WAKO) containing 10% FBS. All cells were cultured at 37°C under 5% CO_2. Cells were treated with 4,5,6,7-tetrabromobenzotriazole (TBB) (2275; Tocris), H89 (CAY10010556; Cayman Chemical), and 8Br-cAMP (201564; Santa Cruz). Cells were rinsed with PBS and exposed to 100 J/m^2 or 25 J/m^2 UV-C in a StrataLinker 1800 crosslinker (Agilent-Stratagene, Santa Clara, CA, USA).

2.2 | Acquisition of GO terms of PIPs

GO annotation was performed using Database for Annotation, Visualization and Integrated Discovery (DAVID) version 6.8.[15,16] The functional annotation table of GOTERM_BP_DIRECT, GOTERM_CC_DIRECT, and GOTERM_MF_DIRECT were obtained. A Venn diagram was generated using the R package VennDiagram[17] (Figure 1).

2.3 | Immunoblotting

For the preparation of the total cell lysates, the collected cells were washed with ice-cold PBS, suspended in sample buffer (2% SDS, 10% glycerol, 100 μmol/L dithiothreitol, 0.1% bromophenol blue, and 50 mmol/L Tris-HCl at pH 6.8), and boiled for 5 min. For the preparation of the whole cell extracts, cells were lysed in immunoprecipitation (IP) kinase buffer (50 mmol/L HEPES pH 8.0, 150 mmol/L NaCl, 2.5 mmol/L EGTA, 1 mmol/L DTT, 0.1% Tween-20, and 10% glycerol). Raw digital images were captured using the ChemiDoc Imaging system (Bio-Rad). The bands of the target protein were quantified using Image Lab (Bio-Rad) or ImageJ, and normalized to that of β-actin, unless stated otherwise. A representative image is shown in the figures.

2.4 | Subcellular fractionation

Subcellular fractionation was performed as previously described.[2] To solubilize the chromatin fraction, pellets were suspended in IP kinase buffer containing a cocktail of protease inhibitors, and the mixture was sonicated. After centrifugation at 17 900 *g* for 10 min, the supernatant was used to solubilize the chromatin fraction.

2.5 | Knockdown experiments by siRNA transfection

HCT116 cells were transfected with either a control siRNA (Silencer Negative Control number 2; Ambion), NIPP1 (M00010903-01; Thermo Scientific) or PNUTS (M011358-00; Thermo Scientific) using Lipofectamine 2000 (11668-027; Invitrogen).

2.6 | CRISPR/Cas9-mediated gene depletion

The *PPP1R8* sgRNA sequence was determined using Integrated DNA Technologies' design custom gRNA tool (https://sg.idtdna.com/site/order/designtool/index/CRISPR_CUSTOM). sgRNA was ordered as oligonucleotides, annealed, and cloned into pX330 (gifted by Dr. KI. Nakayama) with the *Bbs*I site. HeLa and HEK293T cells were cultured at a density of 1 × 10^4 cells/3.5 cm dish for 24 h in DMEM containing 10% FBS. The cells were transfected

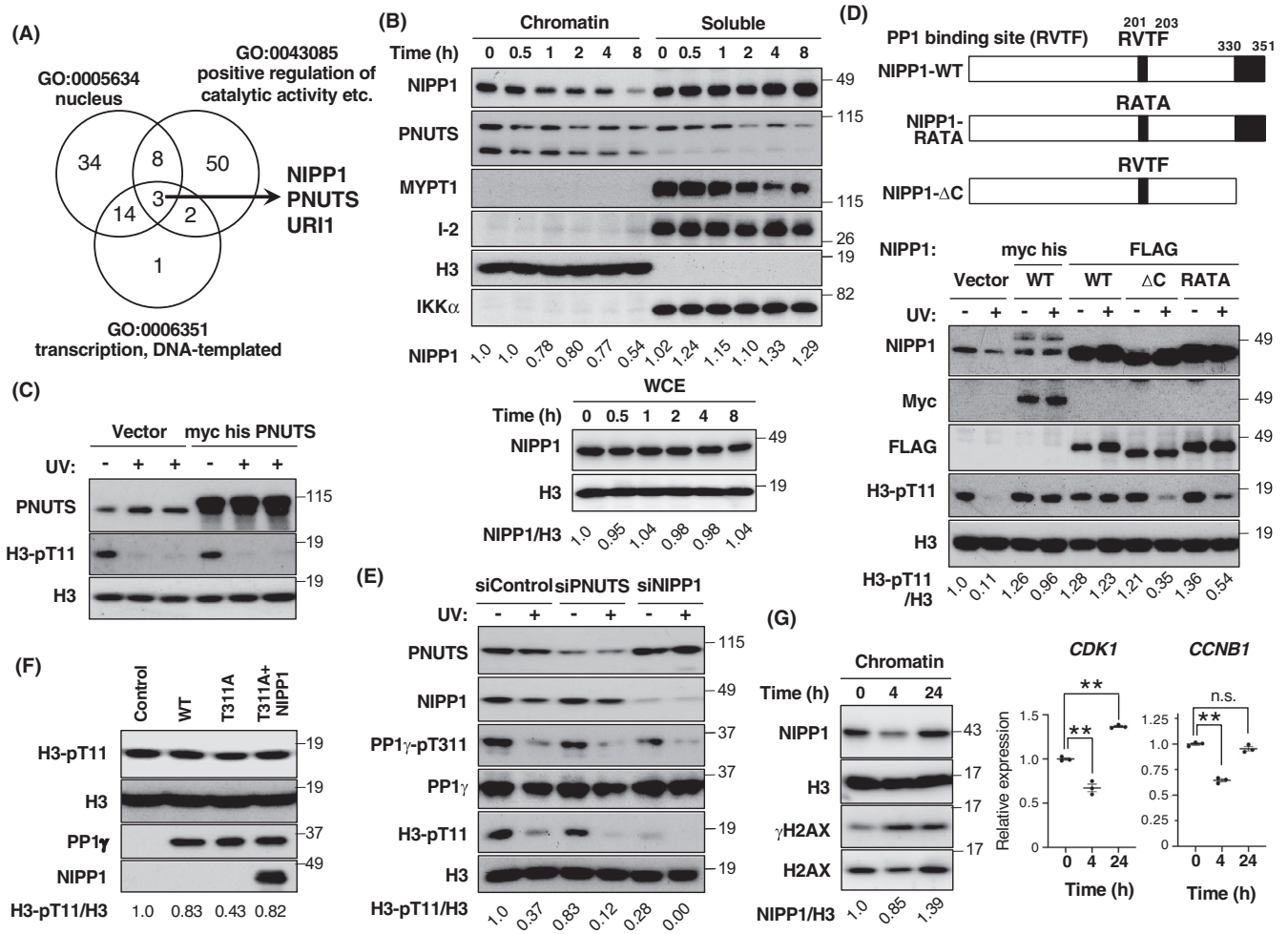

FIGURE 1 NIPP1 inhibited PP1γ activity toward H3-pThr^{11} dephosphorylation. A, Venn diagram showing the number of PIPs that overlap among nucleus (GO:0 005 634), transcription, DNA-templated (GO:0 006 351) and regulators of catalytic activity. Regulators of catalytic activity contain positive regulation of catalytic activity (GO:0 043 085), negative regulation of catalytic activity (GO:0 043 086), negative regulation of phosphatase activity (GO:0 010 923) and positive regulation of phosphoprotein phosphatase activity (GO:0 032 516). B, HCT116 cells were treated with UV and harvested at the indicated times. The chromatin fraction, soluble fraction, and whole cell extract (WCE) were subjected to immunoblotting using the indicated antibodies. IKKα and H3 were used as markers of soluble protein or chromatin protein, respectively. Relative band intensity of NIPP1 (WCE) was normalized by H3, compared with 0 h. Relative band intensity of NIPP1 on chromatin and soluble fractions was normalized by NIPP1 (WCE). Signals were quantified using ImageJ software. C, HCT116 cells were transfected with empty vector or vectors expressing myc-his-PNUTS. After 48 h, the cells were treated with (+) or without (−) UV. The cells were harvested 2 h after treatment and chromatin fractions were subjected to immunoblotting using the indicated antibodies. D, Domain structure of NIPP1-RATA and NIPP1-ΔC mutant are shown. NIPP1 contains PP1-binding region harboring the RVTF sequence (top). HCT116 cells were transfected with empty vector or vectors expressing the indicated NIPP1 (bottom). After 48 h, the cells were treated with (+) or without (−) UV. The cells were harvested 2 h after treatment and chromatin fractions were subjected to immunoblotting using the indicated antibodies. Signals were quantified using Image Lab. E, HCT116 cells were transfected with either control, PNUTS, or NIPP1 siRNAs. After 70 h, the cells were treated with (+) or without (−) UV. Chromatin fractions were prepared for immunoblotting after 2 h incubation. Signals were quantified using Image Lab. F, In vitro phosphatase assay was performed using purified PP1γ and NIPP1. PP1γ-WT, or T311A preincubated with his-NIPP1 were incubated with chromatin. The phosphorylation of H3-Thr^{11} was monitored by immunoblotting using H3-pThr^{11} antibodies. The relative band intensity of H3-pThr^{11} was normalized by H3, compared with the control, and quantified using ImageJ software. G, HCT116 cells were treated with 25 J/m^2 UV and harvested at the indicated times (left). The chromatin fraction was subjected to immunoblotting using the indicated antibodies. H3 was used as markers of chromatin protein. Relative band intensity of NIPP1 was normalized by H3, compared with 0 h. Signals were quantified using Image Lab. Real-time PCR analysis of *CDK1* and *CCNB1* expression in HCT116 cells (right). Data are provided as the mean ± SEM of 3 independent experiments. The results were considered statistically significant at $^*P < .05$ and $^{**}P < .01$ [Correction added on 14 May 2021, after first online publication: Figure 1D has been corrected.]

with 1.4 μg pX330-PPP1R8 and 0.1 μg pPGK-puroR (gifted by Dr. KI. Nakayama) using Polyethylenimine Max (24765-1; Polyscience). At 24 h after transfection, the cells were treated with 1 μg/mL puromycin for 1 d to select the transfected cells. gDNA was extracted from transfected cells using LaboPass Tissue Mini (CME 0111; Cosmo Genetech) and used for the T7 endonuclease

I assay to confirm the cleavage efficiency of sgRNA. After confirmation, the cells were split individually to form a clonal cell line. Immunoblotting and sequencing of gDNA around the target region were performed to confirm gene disruption (sgRNA sequence: sgNIPP1-1; CGCTGTTCGACTGCCCAACC, sgNIPP1-2; GTTCCTGAATCGACCAACTG). For the growth curves, cells were seeded into 3.5 cm dishes at 2.0×10^4 (Figure 2A) or 2.5×10^4 (Figure S2A) cells/dish and counted every 3 d.

2.7 | Quantitative RT-PCR (RT-qPCR) analysis

Total RNA extraction was performed as described previously.[1] Total RNA was extracted using ISOGEN II (311-07361; NIPPON GENE) in accordance with the manufacturer's protocol, and reverse transcription was performed. RNA was reverse-transcribed with random primers using a High Capacity cDNA Reverse Transcription Kit (4368814; ABI). qPCR was performed using FastStart Universal

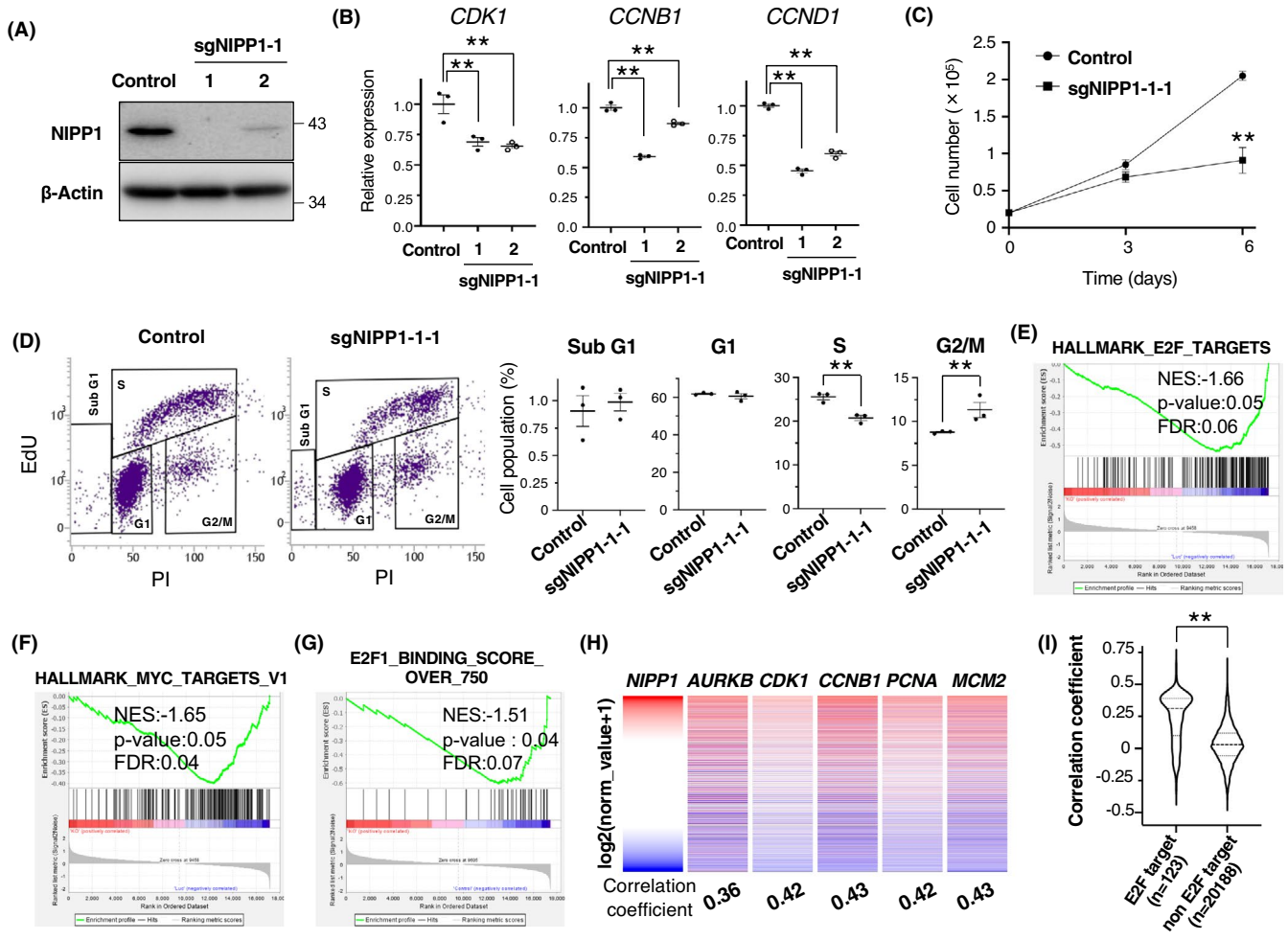

FIGURE 2 NIPP1 is required for the transcription of specific gene functions of E2F target genes. A, Parental and corresponding NIPP1-depleted HeLa cell lines by CRISPR/Cas9 were analyzed by immunoblotting with the indicated antibodies. B, Real-time PCR analysis of *CDK1*, *CCNB1*, and *CCND1* expression in control and NIPP1-depleted HeLa cells. Data are provided as the mean ± SEM of 3 independent experiments. The results were considered statistically significant at $^*P < .05$ and $^{**}P < .01$. C, Control and NIPP1-depleted HeLa cells were cultured and collected, and the cell numbers were counted. Data are provided as the mean ± SE of the mean (SEM) of 3 independent experiments. The results were considered statistically significant at $^*P < .05$ and $^{**}P < .01$. D, Cell cycle distributions of control and NIPP1-depleted HeLa cells were verified by FACS analysis. Each cells were stained with EdU and PI. Fractions of cells in each phase of the cell cycle were quantified. Data are provided as the mean ±SEM of 3 independent experiments. The results were considered statistically significant at $^*P < .05$ and $^{**}P < .01$. E, F, The enrichment plot of HALLMARK_E2F_TARGETS (E) and HALLMARK_MYC_TARGETS_V1 (F) in NIPP1-KO mouse testis compared with NIPP1-WT was generated using GSEA software. NES: normalized enrichment score; FDR: false discovery rate. Four biological replicates were analyzed. G, The enrichment plot of E2F1_BINGING_OVER_750 in NIPP1-KO mouse testis compared with NIPP1-WT was generated using GSEA software. E2F1 target gene set containing E2F1 binding score higher than 750 in E2F target genes (n = 49).[32] NES: normalized enrichment score; FDR: false discovery rate. Four biological replicates were analyzed. H, Pearson's correlation coefficient between NIPP1 and the E2F1 target genes and heat map in TCGA Pan-Cancer dataset (n = 11 060) were calculated using UCSC Xena. I, Violin plot of correlation coefficient between NIPP1 and E2F target (n = 123) or non-E2F target genes (n = 20 188) in TCGA Pan-Cancer dataset (n = 11 060) was calculated using UCSC Xena. The results were considered statistically significant at $^*P < .05$ and $^{**}P < .01$ [Correction added on 14 May 2021, after first online publication: Figures 2A and C have been corrected.]

SYBR Green Master (11226200; Roche) and the StepOnePlus real-time PCR system (Applied Biosystems). Expression levels were normalized to that of glyceraldehyde-3-phosphate dehydrogenase (GAPDH). The following primers were used for amplification in RT-qPCR: CCNB1-F: CAAGCCCAATGGAAACATCT, CCNB1-R: GGATCAGCTCCATCTTCTGC,CCND1-F:GAAGCCCTGCTGGAGTCA, CCND1-R:CCAGGTCCACCTCCTCCT,CDK1-F:TTTTCAGAGCTTTGG GCACT, CDK1-R: AGGCTTCCTGGTTTCCATTT, GAPDH-F: GAGTCA ACGGATTTGGTCGT, GAPDH-R: TTGATTTTGGAGGGATCTCG. All sequences are shown in the 5′→3′ direction.

2.8 | Transient transfection

Here, 4 μg of pcDNA3.1-myc-his-hPP1γ-WT, hPP1γ-T311A, hPNUTS, hNIPP1, pCMV-3×FLAG-ratNIPP1-WT, NIPP1-ΔC, and NIPP1-RATA (gifted by Dr. N. Tanuma) were transfected into HCT116 cells using Lipofectamine 3000 (L3000-008; Invitrogen) or polyethylenimine (24765-1; PSI) transfection reagent, in accordance with the manufacturer's protocol.

2.9 | Mutagenesis

pCMV-3×FLAG-ratNIPP1 S178A and S199A were generated using the KOD-Plus-Mutagenesis Kit (SMK-101,2wq; Toyobo). The following amplification primers were used: S178A-F: GCTACCCTCACT ATTGAAGAGGGAAATC, S178A-R: AATCCGCTTGTTGTGGGC, S199A-F: GCGAGGGTGACCTTCAGTGA, S199A-R: GTTCTTCCTCTT CCTCTTTGGTCT.

2.10 | Lentivirus generation and infection

Lentivirus generation and infection were performed as previously described.[18] Briefly, lentiviruses expressing shControl, shPKAα or shNIPP1 were generated by co-transfection of HEK293T cells with pCMV-VSV-G-RSV-RevB and pCAG-HIVgp (gifted by Dr. H. Miyoshi), and the respective CS-RfA-ETBsd using polyethylenimine. Cells infected with viruses were treated with 10 μg/mL blasticidin (A1113903; Gibco) for 2 d. To express the shRNA, doxycycline (Dox) (D9891; Sigma-Aldrich) was added to the medium at a concentration of 1 μg/mL.

2.11 | Construction of shRNA

To generate lentivirus-based shRNA constructs, a 21-base shRNA-coding fragment with an ACGTGTGCTGTCCGT loop was introduced into pENTR4-H1 digested with *Bam*HI/*Bgl*II. The resulting pENTR4-H1-shRNA vectors were then incubated with CS-RfA-ETBsd vectors and LR Clonase enzyme mix (Invitrogen) for 2 h at 25°C, which produced the CS-RfA-ETBsd-shRNA vector. The target sequences for lentivirus-based shRNA were PKAα: GAAGCTCCCTTCATACCAAAG, NIPP1: GGATTTCTACCCTTACCATTG. For the growth curves, the cells were seeded into 3.5-cm dishes at 2.5×10^4 (Figure S2B) or 1.0×10^5 (Figure S2C) cells/dish and counted every 3 d.

2.12 | Cell cycle analysis

5-Ethynyl-2′-deoxyuridine (EdU) labeling was carried out using the Click-iT Plus EdU Alexa Fluor 488 Imaging kit (C10637; Thermo Scientific). Cells were cultured with 10 nmol/L EdU for 1 h. Harvested cells were fixed with 4% PFA (18814-10; Polysciences) diluted with PBS, for RT and 30 min at 4°C following 10 min at RT. After fixation, cells were washed with 3% BSA (013-27054; Wako) dissolved with PBS. Then incubated with 0.5% Triton-X (168-11805; Wako) diluted with PBS for 20 min at RT. Detection of incorporated EdU was carried out in accordance with the manufacturer's protocol. Cells were treated with RNase, and stained with propidium iodide. Flow cytometry was performed using a FACSVerse flow cytometer (BD Biosciences). Cell cycle profile was analyzed using BD FACSDiva™ software (BD Biosciences).

2.13 | Chromatin immunoprecipitation assay

HCT116 cells were synchronized with nocodazole (50 ng/mL, 12 h), and mitotically arrested cells were collected by shaking. At 7 h after release, the cells synchronized at early S phase confirmed by FACS were irradiated with or without 100 J/m^2 UV and incubated for an additional 2 h. These cells were fixed, and ChIP assays were performed as previously described.[1] Quantitative real-time PCR reactions were performed on an ABI 7500 Fast instrument. The SYBR Green PCR Master Mix (Applied Biosystems) was used to detect all products. The percentage of chromatin IP toward the total chromatin input was analyzed and expressed as fold enrichment after UV irradiation.

2.14 | Phosphatase assay

An in vitro phosphatase assay was performed as described previously.[2] Briefly, chromatin-bound PP1γ was solubilized and immunoprecipitated with a PP1γ antibody. The precipitates were incubated with chromatin at 30°C for 1 h in phosphatase buffer (10 mmol/L HEPES, 10 mmol/L $MgCl_2$, 1 mmol/L $MnCl_2$, and 1 mmol/L DTT). His-tagged wild-type PP1γ, PP1γ–T311A and NIPP1 were purified from Sf9 cells and phosphatase assays were performed using a chromatin fraction as a substrate.

2.15 | Antibodies

The antibodies used for immunoblotting or ChIP were Chk1 (sc8408 and sc56291; Santa Cruz), FLAG (M158-3L; MBL), myc (sc789 and

sc40; Santa Cruz), H3 (ab1791; Abcam), I-2 (AF4719; R&D SYSTEMS), IKKα (sc7182; Santa Cruz), NIPP1 (612368; BD Biosciences; HPA027452; Sigma), normal goat IgG (sc2028; Santa Cruz), normal mouse IgG (sc2025; Santa Cruz), normal rabbit IgG (cs2729; Cell Signaling), PKAα (sc28315; Santa Cruz), PKA-pThr^{197} (cs4781; Cell Signaling), pS/T-PKA (cs9624; Cell Signaling), H2AX (ab11175; Abcam), γH2AX (05-636; Sigma), H3 (17168-1-AP; Proteintech), H3-pThr^{11} (ab5168; Abcam), PNUTS (611060; BD Biosciences), PP1-pThr^{321} (2581; Cell Signaling; Thr^{321} corresponds to Thr^{311} of PP1γ), PP1γ (sc6108; Santa Cruz; 07-1298; Millipore), and MYPT1 (ab59235; Abcam).

2.16 | Statistical analysis

To compare 2 groups, two-sided Student *t* test (Figures 2C,D, 5, and S2B,C) or Welch *t* test (Figures 2I and 6) were used. To compare 3 or more groups, one-way ANOVA followed by Tukey multiple comparison test (Figures 1G, 3C,D, and S2A) or Dunnett multiple comparisons test (Figures 2B and S4) was chosen for multiple comparisons. Results were considered statistically significant at $^{*}P < .05$, $^{**}P < .01$. Statistical analyses were performed using GraphPad Prism 6 (GraphPad Software, Inc, San Diego, CA).

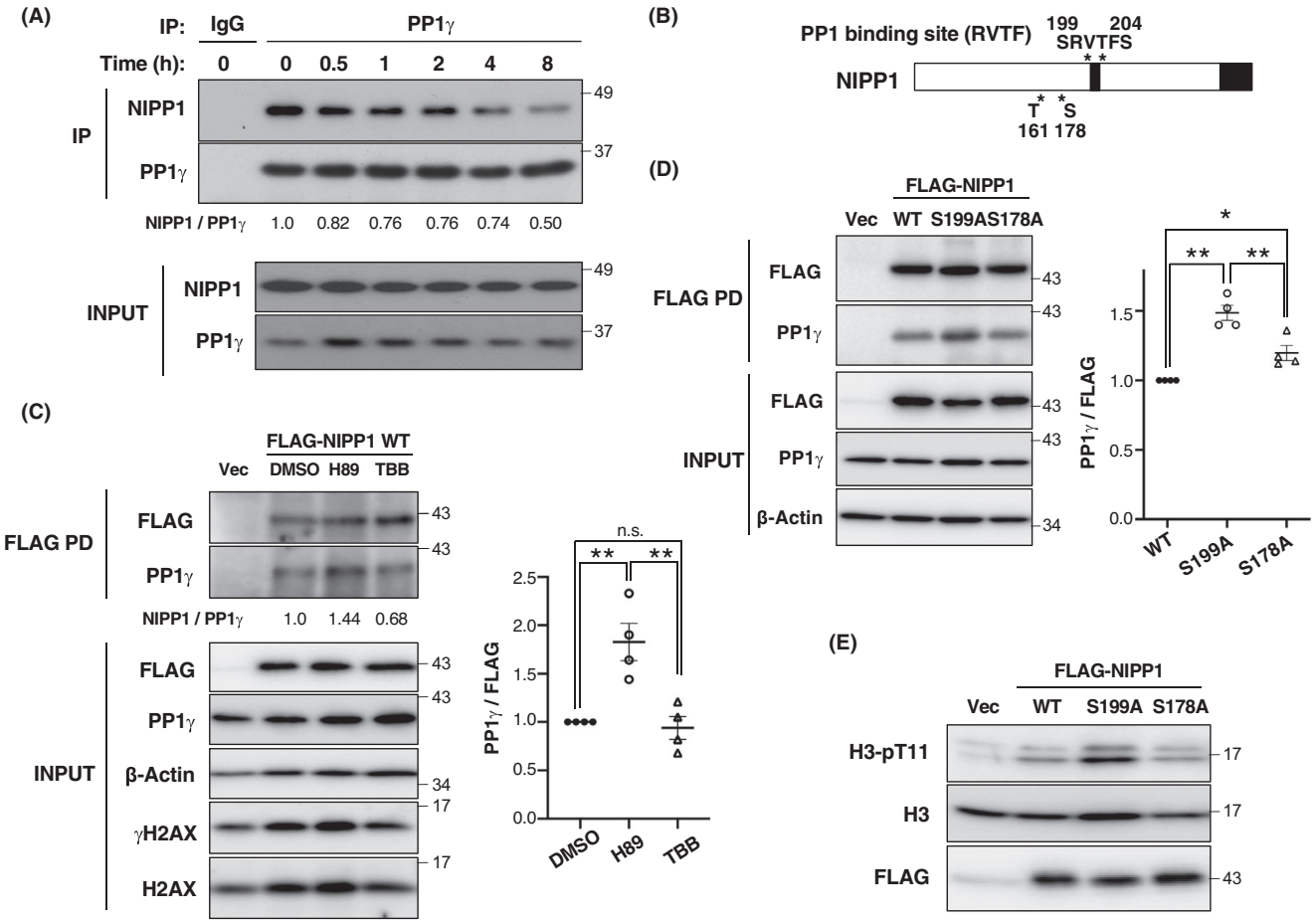

FIGURE 3 Phosphorylation of NIPP1 is important for the release of PP1γ A, Chromatin fractions from UV-irradiated HCT116 cells were solubilized as shown in Materials and Methods and subjected to IP-western analysis using the indicated antibodies. IgG was used as a negative control. The relative band intensity of NIPP1 was normalized by PP1γ. The results are shown compared with 0 h. Signals were quantified using Image J software. B, Domain structure and phosphorylation sites mediated by PKA and CK2 of NIPP1 are shown. NIPP1 contains PP1-binding region harboring RVTF sequence. C, HCT116 cells were treated with TBB (50 μmol/L) or H89 (40 μmol/L) and irradiated with UV light. After 4 h, the cells were collected and the chromatin fractions were solubilized and subjected to pulldown with FLAG M2 agarose. Immunoblotting was performed using the indicated antibodies. The relative band intensity of PP1γ was quantified using Image Lab and normalized by that of FLAG-NIPP1, compared with DMSO (n = 4). The results were considered statistically significant at $^{*}P < .05$ and $^{**}P < .01$. D, HCT116 cells were transiently transfected with NIPP1-WT, NIPP1-S178A, or NIPP1-S199A, lysed, and subjected to pulldown with FLAG M2 agarose. Immunoblotting was performed using the indicated antibodies. The relative band intensity of PP1γ was quantified using Image Lab and normalized by that of FLAG-NIPP1, compared with NIPP1-WT (n = 4). The results were considered statistically significant at $^{*}P < .05$ and $^{**}P < .01$. E, HCT116 cells were transiently transfected with NIPP1-WT, NIPP1-S178A, or NIPP1-S199A, lysed, and subjected to immunoblotting using the indicated antibodies

2.17 | Bioinformatics analysis

Publicly available RNA-seq data for NIPP1-control and NIPP1-KO mouse testes were obtained from Gene Expression Omnibus (GEO) under accession number GSE83145.[19] After adapter sequences were trimmed from reads using Trim Galore! version 0.6.4,[20] quality control and filtering were performed using PRINSEQ version 0.20.4.[21] Reads were aligned to the reference genome *Mus musculus* (GRCm38.98) [22-25] and counted per transcript using Salmon version 0.14.2.[26] Toximport version 1.12.3[27] summarized transcript-level estimates for gene-level analysis. Gene set enrichment analysis (GSEA) was carried out with Signal2Noise values for all detected genes for the indicated comparisons as the ranking metric using GSEA software version 4.0.3,[28] hallmark version 7.0 (Figure 2E,F).[29] We created a custom gene set (E2F1_BINDING_SCORE_OVER_750) as the gene set database to be tested for enrichment. In total, 41 genes were included in E2F1_BINDING_SCORE_OVER_750 (Figure 2G). Publicly available RNA-seq data for the control and PKA inhibitor (H89)-treated 3T3 cells were

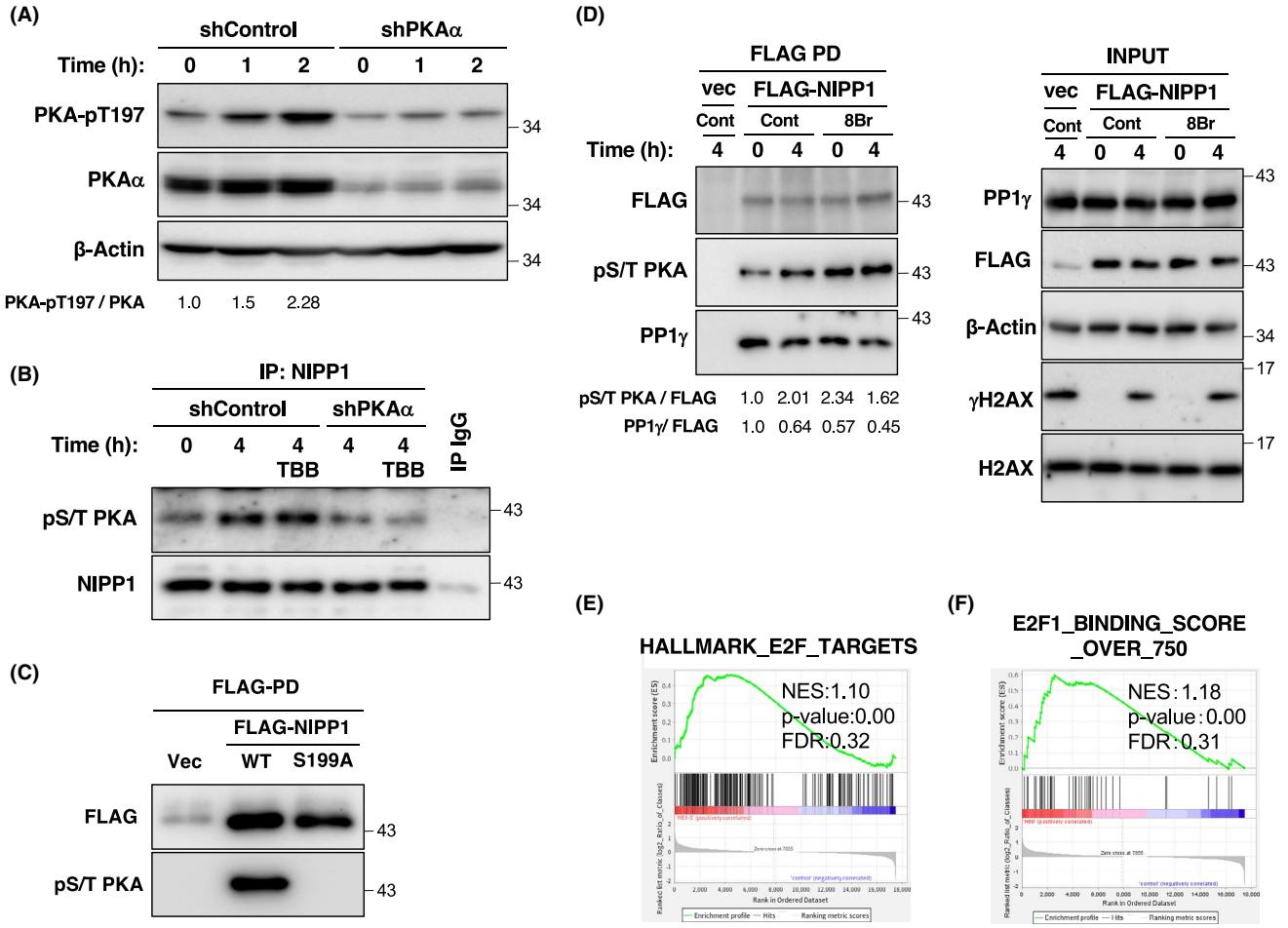

FIGURE 4 PKA regulates the interaction between NIPP1 and PP1γ. A, HCT116 cells were cultured in the presence of Dox for 3 d to knockdown PKAα or luciferase (shControl) using tetracycline-inducible shRNA and irradiated with UV. After the indicated times, the cells were collected and the total cell extracts were subjected to immunoblotting using the indicated antibodies. Signals were quantified using Image Lab. B, HCT116 cells expressing shControl or shPKAα were cultured with or without TBB, and treated with or without UV for 4 h. NIPP1 was immunoprecipitated from the total cell extracts and immunoblotted with an anti-phospho-S/T-PKA substrate and anti-NIPP1 antibodies. IgG was used as a negative control. C, HCT116 cells were transiently transfected with NIPP1-WT or NIPP1-S199A and cultured for 2 d. After irradiation with UV for 4 h, the cells were lysed and subjected to pulldown with FLAG M2 agarose. Immunoblotting was performed using the indicated antibodies. D, HCT116 cells were transfected with FLAG-NIPP1 and cultured for 2 d. The cells were treated with 8Br-cAMP (500 μmol/L) for 2 h and irradiated with UV. After 4 h, the total cell extracts were subjected to pulldown with FLAG M2 agarose. Samples were immunoblotted with the indicated antibodies. The relative band intensity of PP1γ and pS/T-PKA was quantified using Image Lab and normalized to that of FLAG compared with control. E, An enrichment plot of HALLMARK_E2F_TARGETS in mouse 3T3 cells treated with H89 for 3 h compared with untreated 3T3 cells was generated using GSEA software. NES: normalized enrichment score; FDR: false discovery rate. Two biological replicates were analyzed. F, An enrichment plot of E2F1_BINDING_SCORE_ OVER_750 in mouse 3T3 cells treated with H89 for 3 h compared with untreated 3T3 cells was generated by GSEA software. E2F1 target gene set containing E2F1 binding scores higher than 750 in E2F target genes (n = 49).[32] NES: normalized enrichment score; FDR: false discovery rate. Two biological replicates were analyzed [Correction added on 14 May 2021, after first online publication: Figure 4C has been corrected.]

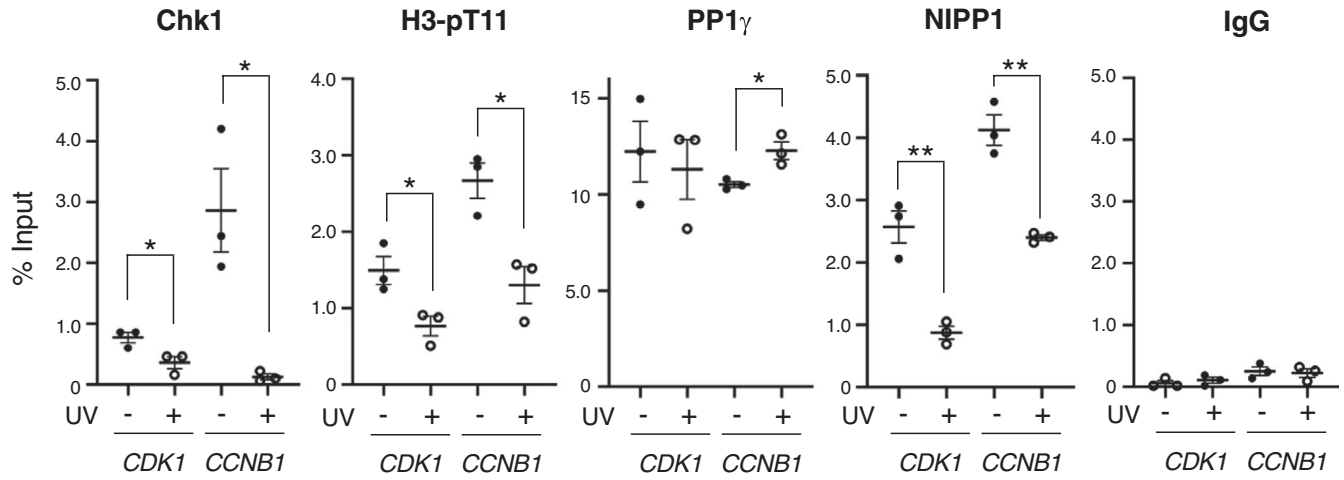

FIGURE 5 Dynamic changes in promoter occupancy at E2F promoters within *CDK1* and *CCNB1*. ChIP assays were performed using G1/S synchronized HCT116 cells, as described in Materials and Methods. The results are shown as fold enrichment expressed as a percentage of the total input chromatin. Data are provided as the mean ± SEM of at least 3 independent experiments. The results were considered statistically significant at $^{*}P < .05$ and $^{**}P < .01$

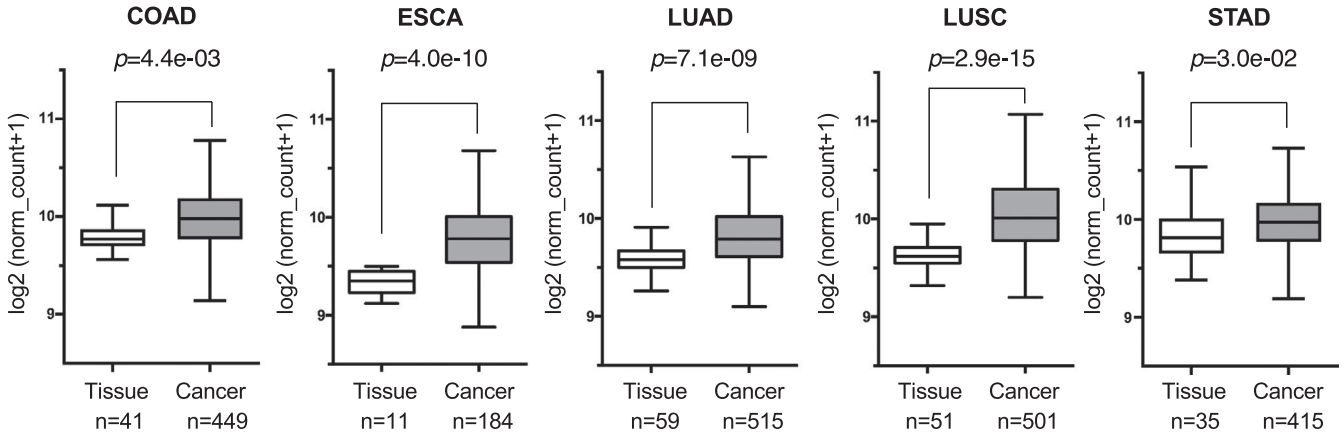

FIGURE 6 NIPP1 mRNA expression is upregulated in several cancers. The NIPP1 mRNA expression levels in normal solid tissue and primary tumors of each cancer type dataset in TCGA were obtained using UCSC Xena. The fold-change was calculated using the median. Data for the top 5 upregulated cancer types are shown. In the box plot, the central line reflects the median, while the borders of the boxes show the interquartile range of the plotted data. The whiskers extend to 1.5-fold the interquartile range, and outliers are not shown

obtained from GEO under accession number GSE58746.[30] Data analysis was performed as described above. TPM+1 was used as the expression value, and GSEA was carried out with log2_Ratio_of_Classes (Figure 4E,F).

2.18 | NIPP1 expression analysis

mRNA expression data were obtained from The Cancer Genome Atlas (TCGA) at the University of California at Santa Cruz (UCSC) Cancer Genomics Browser (http://xena.ucsc.edu/). The difference in NIPP1 expression between primary tumor and solid tissue normal was determined using the BLCA, BRCA, CHOL, COAD, ESCA, HNSC, KICH, KIRC, KIRP, LIHC, LUAD, LUSC, PRAD, READ, STAD, THCA, and UCEC datasets from TCGA obtained via UCSC, as stated above. These abbreviations for the cancer types are based on TCGA study abbreviation. To perform appropriate statistical analysis, datasets containing 5 or more solid tissue normal samples were analyzed (Figure 6). Box plot figures were generated for the top 5 upregulated cancer types using GraphPad Prism Version 6 (GraphPad Software, Inc, San Diego, CA).

2.19 | E2F1 targets and NIPP1 expression analysis

mRNA expression data was obtained from TCGA Pan-Cancer (PANCAN) dataset (Batch effects normalized mRNA data; n = 11 060) via UCSC Xena (http://xena.ucsc.edu/).[31] Pearson's correlation coefficient of mRNA expression between *NIPP1* and all other genes was calculated using all patient, including primary tumor, metastasis, and solid tissue normal, data in TCGA PANCAN. A heatmap was generated using UCSC Xena (Figure 2H)[31] and a violin plot was

generated using GraphPad Prism Version 6 (GraphPad Software, Inc, San Diego, CA) (Figure 2I).

2.20 | ChIP-Atlas database analysis

E2F target genes were obtained from a previous study,[32] and the E2F1 binding score was obtained using ChIP-Atlas.[33] The search parameters were as follows: antigen, E2F1; species, *H sapiens*; distance from TSS, ±1 kb. All databases except for SRX1556104 and SRX1556105 were used. SRX1556104 and SRX1556105 were excluded because the binding scores of all E2F1 target genes were zero (n = 49). The E2F1 target gene set was considered at an E2F1 binding score higher than 750 in E2F target genes (Figures 2G and 4F). Additional experimental methods are described in Appendix S1.

3 | RESULTS

3.1 | NIPP1 is a regulatory protein that inhibits DNA damage-induced dephosphorylation of H3-pThr^{11}

We explored the regulatory subunit(s) involved in transcriptional regulation by evaluating the PP1γ-mediated histone H3 dephosphorylation at Thr^{11}. As mentioned above, the enzymatic activity of PP1 is regulated by its binding to regulatory subunits.[6] To select PP1 interacting proteins (PIPs) that could be potentially involved in dephosphorylation of H3-pThr^{11} from nearly 200 known PIPs, we focused on 3 categories: PIPs located in the nucleus, where histones are mainly located (GO:0005634—nucleus); PIPs involved in transcription (GO:0006351—transcription, DNA-templated); PIPs implicated in the modulation of PP1 activity (GO:0043085—positive regulation of catalytic activity, GO:0043086—negative regulation of catalytic activity, GO:0010923—negative regulation of phosphatase activity, and GO:0032516—positive regulation of phosphoprotein phosphatase activity). We obtained genes that annotated these GO terms, including regulatory subunits of PP1,[34] and identified 3 genes which satisfied these conditions; *PPP1R8* (NIPP1, nuclear inhibitor of PP1), *PPP1R10* (PNUTS, phosphatase 1 nuclear targeting subunit), and *URI1* (unconventional prefoldin RPB5 interactor 1) (Figure 1A). Importantly, NIPP1 and PNUTS have also been reported to be involved in DNA damage responses.[35,36] Therefore, we focused on these 2 molecules and examined the effect of PP1γ on the dephosphorylation of H3-pThr^{11}.

NIPP1 has been found to be a potent inhibitor and a major nuclear interactor of PP1,[9] while PNUTS plays multiple roles in several cellular processes, including cell cycle progression, DNA repair, and apoptosis, by regulating the activity of PP1.[37,38] To determine whether NIPP1 or PNUTS were involved in PP1γ-dependent H3-Thr^{11} dephosphorylation, we first examined whether NIPP1 and PNUTS were localized to the chromatin. Both were detected in the chromatin and soluble fractions, whereas other PP1-regulatory subunits (MYPT1 and I-2) were predominantly detected in soluble fractions (Figure 1B). After UV irradiation, chromatin-bound NIPP1 decreased, while soluble NIPP1 increased, suggesting that NIPP1 translocated from the chromatin to the soluble fraction upon DNA damage (Figure 1B). Next, we found that the overexpression of NIPP1-WT (myc-his-or FLAG-tagged NIPP1), but not PNUTS, resulted in increased H3-pThr^{11} upon DNA damage (Figure 1C,D). C-terminally truncated NIPP1 (NIPP1-ΔC) lacks the 22 amino acids of the C-terminal that function as inhibitors of PP1.[10] Therefore, NIPP1-ΔC forms a hyperactive holoenzyme with PP1. While the overexpression of NIPP1-WT inhibited the dephosphorylation of H3-pThr^{11} upon DNA damage, H3-pThr^{11} was dephosphorylated in NIPP1-ΔC-overexpressed cells (Figure 1D). NIPP1 contains an RVxF motif, which is present in approximately 90% of validated PP1-interacting proteins.[34] Therefore, we investigated the effect of H3-pThr^{11} by overexpressing a NIPP1 mutant that does not bind PP1 (NIPP1-RATA: Val^{201} and Phe^{203} to Ala mutant). We found that the effect of NIPP1 overexpression appeared to be directly dependent on its binding to PP1 as NIPP1-RATA failed to suppress DNA damage-induced H3-Thr^{11} dephosphorylation (Figure 1D). Conversely, the depletion of NIPP1 by siRNA resulted in a reduction in the phosphorylation of H3-Thr^{11}, even in the absence of DNA damage (Figure 1E). This reduction was not observed when the PNUTS was depleted. Consistent with the inhibitory role of NIPP1 in PP1γ, the knockdown of NIPP1 decreased the phosphorylation of PP1γ at Thr^{311}, suggesting that PP1γ is active in NIPP1-depleted cells. Furthermore, using an in vitro phosphatase assay, we found that NIPP1 suppressed the dephosphorylation activity of PP1γ against H3-pThr^{11} (Figure 1F). Of note, we found the chromatin binding of NIPP1 and the expression of E2F1 target genes, such as *CDK1* and *CCNB1*, were correlated at 4 h and 24 h after UV irradiation (Figure 1G). These results suggested that PP1γ activity was regulated in response to DNA damage by at least 2 distinct mechanisms: the first involving Cdk-dependent PP1γ-Thr^{311} phosphorylation[2] and the second involving NIPP1 binding.

3.2 | CRISPR/Cas9-mediated depletion of NIPP1 shows growth defects with decreased E2F target gene expression

To determine whether NIPP1 exerts physiological roles in transcription and cell proliferation, NIPP1-depleted HeLa cells were generated by CRISPR/Cas9-mediated double-strand break without donor. We used HeLa cells to deplete NIPP1 because NIPP1-depleted HCT116 cells did not efficiently proliferate when they were single cells. We confirmed by immunoblotting that NIPP1 protein levels were almost undetectable (Figure 2A). In addition, NIPP1-depleted cells harbored CRISPR/Cas9-induced InDels (Figure S1) at the sgRNA target site on *PPP1R8* locus. We found that expression of E2F target genes was reduced in NIPP1-depleted cells (Figure 2B). NIPP1-depleted cells showed a reduced proliferation ability compared with the control parental cells (Figure 2C). We analyzed the cell cycle profiles by pulse labeling with EdU, in addition to PI staining. This assay revealed that the

population of cells in the S phase of the cell cycle was decreased in sgNIPP1 cells, whereas that in G2/M phase was increased (Figure 2D). To exclude the possibility that these findings resulted from clonal variance, we established 2 independent sgRNA targets of HEK293T cells in which NIPP1 was depleted by sgNIPP1, and found that the proliferation of these cells was also attenuated by the loss of NIPP1 (Figures S2A and S3). We also performed shRNA-mediated depletion of NIPP1 in HeLa and HCT116 cells. NIPP1 depletion indeed resulted in attenuated cell proliferation compared with control cells (Figure S2B,C). These results were supported by a previous study, which showed that NIPP1 is required for cell proliferation.[19]

Furthermore, we performed GSEA using publicly available RNA-seq data using control and NIPP1 knockout testis,[19] and found a significant enrichment of only 2 gene sets, E2F targets and MYC targets, as downregulated genes in NIPP1 KO (Figure 2E,F). E2F transcription factors include 9 members, showing both distinct and overlapping functions. Among these, E2F1 acts as a master regulator for the activator of G1/S progression. To determine whether NIPP1 regulates E2F1 target genes, we created a set of E2F1 targets with E2F1 binding scores higher than 750 in E2F target genes[32] and performed GSEA using RNA-seq data of NIPP1 KO cells.[19] We found that E2F1 binding genes among the 9 members were significantly reduced in NIPP1 KO mouse testis (Figure 2G). These results provided further support to the notion that NIPP1 is important for the expression of E2F target genes through the inhibition of PP1γ activity.

3.3 | NIPP1 expression correlated with E2F target genes, specifically belonging to G1/S, S/G2, DNA synthesis and replication

Generally, E2F target genes are classified mainly as cell cycle (G1, G1/S, and S/G2), DNA synthesis and replication, negative regulators of the cell cycle, checkpoint, DNA damage repair, apoptosis, development, and differentiation.[32] By calculating the correlation values between NIPP1 mRNA expression and classified E2F target groups, we found that the correlation coefficients of E2F targets belonging to G1/S, S/G2, and DNA synthesis and replication showed values between 0.3 and 0.4, indicating that the expression of NIPP1 and E2F targets is weakly correlated, compared with G1, apoptosis, development, and differentiation (Figure S4A). These results suggested that E2F target genes, particularly in G1/S, S/G2, and DNA synthesis and replication, might be regulated by NIPP1. Furthermore, the correlation coefficients between the expression levels of *NIPP1* and typical targets of E2F1 were calculated. We found that the expression of E2F target genes that contribute to cell cycle regulation, such as *AURKB*, *CDK1*, *CCNB1*, *PCNA*, and *MCM2*, showed significantly higher correlation coefficients (Figure 2H), than those calculated between non-E2F targets (Figure 2I). These results suggested that expression of *NIPP1* was associated with the transcription of E2F1 target genes involved in the cell cycle.

3.4 | PKA-mediated phosphorylation of NIPP1 is important for UV-induced PP1-NIPP1 dissociation

As PP1γ is negatively regulated by NIPP1, we evaluated whether the stability of the PP1γ-NIPP1 complex was affected by DNA damage. NIPP1 translocated from the chromatin to the soluble fraction upon UV irradiation (Figure 1B). We fractionated chromatin and performed PP1γ immunoprecipitation in unirradiated and irradiated cells. We found that the interaction of NIPP1 with PP1γ decreased gradually in the irradiated cells (Figure 3A). These data suggested that PP1γ was released from NIPP1 and activated after DNA damage.

To elucidate the molecular mechanism underlying the destabilization of PP1γ in the NIPP1 complex, we focused on a study showing that the inhibitory function of NIPP1 toward PP1 was suppressed by its phosphorylation by PKA and/or CK2.[14] The same study also found that the phosphorylation sites for PKA (Ser^{199}) and CK2 (Ser^{204}) flanked the RVxF motif of NIPP1 (Figure 3B). Based on this previous finding, we investigated whether PKA or CK2 regulated the interaction of NIPP1 with PP1γ. We used PKA-specific or CK2-specific inhibitors, H89 or TBB, respectively, and found that H89 prevented the release of NIPP1 from PP1γ after DNA damage (Figure 3C), suggesting that PKA regulates the interaction of NIPP1 and PP1γ.

Notably, NIPP1 contains 2 phosphorylation sites, Ser^{178}, and Ser^{199}, mediated by PKA.[14] HCT116 cells were transiently transfected with FLAG-tagged constructs expressing wild-type (WT), Ser^{199}-to-Ala (S199A), or Ser^{178}-to-Ala (S178A) of NIPP1, and irradiated UV. The exogenous FLAG-tagged NIPP1 was immunoprecipitated, and the proteins were probed with anti-FLAG or anti-PP1γ antibodies. As a result, the binding of NIPP1-S199A to PP1γ upon DNA damage was found to be significantly higher than that of NIPP1-WT (Figure 3D). These findings demonstrated that PKA-mediated NIPP1 phosphorylation at Ser^{199}, an adjacent PP1 binding motif, is required for the dissociation of PP1γ from the NIPP1 complex in response to UV-induced DNA damage. We previously reported that the phosphorylation of PP1γ at Thr^{311} inhibited PP1γ activity.[2] These results prompted us to investigate whether PP1γ-Thr^{311} phosphorylation affected the binding of PP1γ to NIPP1. However, the substitution of Thr^{311} with an alanine (T311A) did not affect the interaction of PP1γ with NIPP1 (Figure S5), indicating that the activity of PP1 did not affect its binding to NIPP1.

As shown in Figure 3E, NIPP1-S199A expression enhanced H3-pThr^{11}, in comparison with NIPP1-WT, indicating that NIPP1-S199A inhibited PP1γ activity toward H3-pThr^{11} more effectively than NIPP1-WT. Taken together, these results indicated that the UV-induced phosphorylation of NIPP1 at Ser^{199}, mediated by PKA,

contributed to the dissociation of NIPP1 from PP1γ, and thereby led to PP1γ activation.

3.5 | PKA regulates the interaction between NIPP1 and PP1γ

To determine whether the activity of PKA was regulated by UV irradiation, we monitored the phosphorylation of PKA at Thr[197], which represents the fully activated form of PKA.[39] We found that UV irradiation indeed increased PKA phosphorylation at Thr[197], indicating that UV irradiation activates PKA (Figure 4A), as reported previously.[40] To investigate whether NIPP1 is phosphorylated by PKA after DNA damage, we immunoprecipitated NIPP1 and performed immunoblotting using antibodies against phospho-PKA substrate, which recognizes the consensus PKA target motif, namely, R-x-x-pS/T. We were able to detect NIPP1 by this PKA consensus phospho-antibody upon UV irradiation in shControl cells, but not in shPKAα, one of the isoforms of PKA, cells (Figure 4B). TBB treatment did not affect this phosphorylation. These results indicated that NIPP1 phosphorylation was mediated by PKAα and increased upon DNA damage. To confirm that the PKA consensus phosphor-antibodies could detect NIPP1-Ser[199] in vivo, we expressed FLAG-tagged wild-type NIPP1 or S199A and performed UV irradiation. Phospho-specific signals were detected for NIPP1-WT, but not for NIPP1-S199A, indicating that Ser[199] was phosphorylated upon UV irradiation (Figure 4C). Next, we treated the cells with 8Br-cAMP, which is a PKA activator, and examined the PKA phosphorylation status of NIPP1. We found that 8Br-cAMP treatment increased the phosphorylation of NIPP1 at the PKA consensus site (Figure 4D). Importantly, we also found that the interaction between NIPP1 and PP1γ was reduced by the activation of PKA with 8Br-cAMP, even in the absence of DNA damage (Figure 4D). Taken together, these results suggested that the phosphorylation of NIPP1 by PKA negatively regulates the interaction of NIPP1 with PP1γ.

3.6 | Expression of PKA catalytic subunit is negatively related to specific E2F target genes

To clarify whether PKA is involved in the expression of E2F target genes, we analyzed the RNA-seq data from cells treated with a PKA inhibitor (H89).[30] Expression of E2F target genes was increased in the H89-treated cells compared with the control cells, indicating that PKA may negatively regulate E2F target genes (Figure 4E). We also found that E2F1 binding genes among 9 members of the E2F family significantly increased in H89-treated cells (Figure 4F). Furthermore, we investigated the correlation coefficient between PKA (PKA catalytic subunit; *PRKACA* and *PRKACB*) and the expression of classified E2F target genes. Although there were no significant differences between *PRKACA* and E2F targets, *PRKACB* was negatively associated with the expression of E2F target genes, G1/S, S/G2, and DNA synthesis and replication toward G1, negative regulators of cell cycle and development (Figure S4B,C). These results suggested that PKA functions upstream of NIPP1 and influences the expression of E2F target genes, most likely to be via NIPP1 phosphorylation.

3.7 | The binding of NIPP1 to the E2F target promoters is reduced upon DNA damage

E2F target genes, such as *CDK1* and *CCNB1*, are transcriptionally repressed upon DNA damage in a Chk1-dependent manner.[1] Therefore, we investigated whether PP1γ, or NIPP1 was enriched in the promoter regions of the E2F target genes upon DNA damage. However, the occupancy of E2F proteins at their target gene promoters is known to vary during the cell cycle,[41-43] which is consistent with the notion that E2F-regulated genes are transcriptionally active during the S phase.[44] We, therefore, synchronized HCT116 cells at early S phase and performed ChIP, followed by quantitative PCR analysis, in the presence or absence of DNA damage, using primers flanking potential E2F-binding site(s) within the *CDK1* and *CCNB1* genes. Chk1 was released from these regions, concomitant with a reduction in H3-Thr[11] phosphorylation, as reported previously (Figure 5).[1] In contrast, the association of PP1γ at these promoter regions did not change markedly after DNA damage. PP1γ activity appeared to be regulated by its binding to NIPP1, as shown in Figure 1. We found that the binding of NIPP1 was reduced at these promoters upon UV irradiation. These findings revealed a mechanism for the transcriptional repression of E2F target genes upon DNA damage, due to reduced binding of NIPP1 or Chk1 at these gene promoters, resulting in PP1γ activation.

3.8 | NIPP1 mRNA expression is upregulated in several cancers

As the E2F pathway is frequently deregulated in cancer, we evaluated the correlation between NIPP1 expression and cancer. We examined global changes in gene expression between tumor tissues (cancer) and adjacent nontumor tissues (tissue) using TCGA database, a comprehensive and coordinated resource. As a result, NIPP1 was found to be significantly overexpressed in the colon adenocarcinoma (COAD), esophageal carcinoma (ESCA), lung adenocarcinoma (LUAD), lung squamous cell carcinoma (LUSC), and stomach adenocarcinoma (STAD) groups. (Figure 6). These results indicated an association between NIPP1 and cancer cell proliferation in these types of cancer.

4 | DISCUSSION

Our results revealed a complex signaling pathway for the regulation of transcriptional repression via H3-pThr[11] dephosphorylation upon DNA damage (Figure 7). Under normal conditions, PP1γ

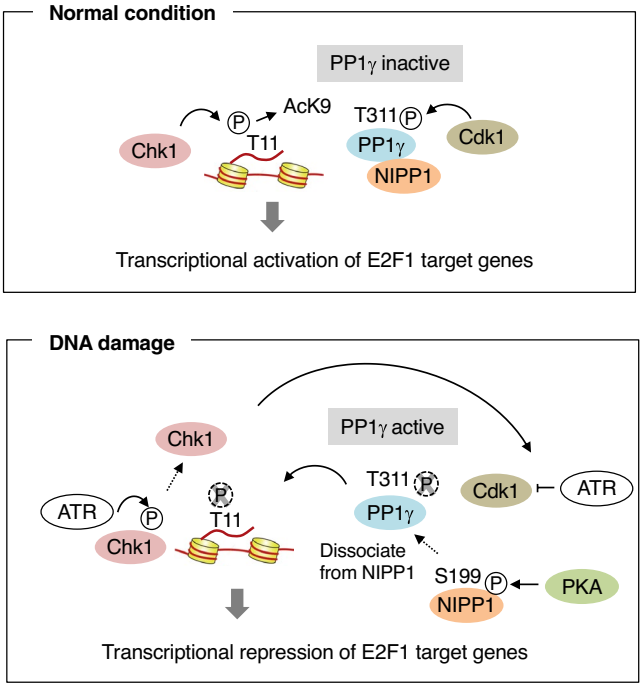

FIGURE 7 Schematic model of DNA damage-induced transcriptional repression of E2F target genes. Under normal conditions, Chk1 phosphorylates H3-pThr^{11}, which induces K9 acetylation, leading to transcriptional activation of E2F1 target genes. PP1γ is inactivated through both Cdk-dependent phosphorylation at pThr^{311} and binding to NIPP1. In response to DNA damage, the ATR-dependent release of Chk1 from chromatin indirectly suppresses Cdk activity, which results in the activation of PP1γ via a reduction in Thr^{311} phosphorylation, and its release from NIPP1 is mediated by PKA phosphorylation. Activated PP1γ dephosphorylates H3-pThr^{11} in collaboration with Chk1 released from E2F1, ultimately resulting in the transcriptional repression of genes, such as *CDK1* and *CCNB1*, involved in the cell cycle

is located on the promoter region of *CDK1* and *CCNB1* genes but does not show activity toward H3-pThr^{11} because it remains in a complex with NIPP1. This allows for H3-Thr^{11} phosphorylation, mediated mainly by Chk1, and in turn for the activation of E2F1 target genes. Upon DNA damage, the amount of PP1γ is not changed, however PP1γ is activated as a result of a reduction of PP1γ-Thr^{311} phosphorylation due to reduced Cdk1 activity.[2] The dissociation of the PP1γ–NIPP1 complex also plays a role in PP1γ activation. Then, activated PP1γ dephosphorylates H3-pThr^{11}, leading to the transcriptional repression of E2F1 target genes. We found that Thr^{311} dephosphorylation did not play a role in PP1γ-NIPP1 dissociation, indicating that phosphorylation by Cdk1 has no effect on binding with NIPP1.

Several studies have shown that NIPP1 binding to PP1 is regulated by the PKA-dependent phosphorylation of Ser^{178} and Ser^{199} and CK2-dependent phosphorylation of Thr^{161} and Ser^{204}.[11,13] The combined phosphorylation of these 4 residues by PKA and CK2 converts NIPP1, which dissociates from PP1, thereby leading to PP1 activation.[11,13,14] We also found that DNA damage increased PKA activity, which is consistent with a previous report showing that UV irradiation activates melanocortin 1 receptor (MC1R) following the upregulation of adenylate cyclase and activation of PKA.[40] The PKA-mediated phosphorylation of NIPP1 at Ser^{199} increased upon DNA damage, triggering the dissociation of PP1γ and NIPP1. After its dissociation from NIPP1, PP1 initiated auto-dephosphorylation, which eventually converted PP1 into its fully active state. Therefore, our study elucidates a novel pathway that links PKA, NIPP1, and PP1 in the cellular response to DNA damage.

PP1 catalyzes phospho-serine/threonine dephosphorylation reactions with various PIPs that determine the activity and selectivity of the phosphatase. Several PIPs have been reported to be involved in regulating PP1 activity during cell cycle and DNA damage responses. For example, Repo-Man is a regulator of PP1 toward mitotic histone H3, but H3-pThr^{11} is unlikely to be a direct substrate of this complex.[45] Inhibitor 2 (I-2), which inhibits PP1, is phosphorylated at Ser^{44} by ATM upon DNA damage, leading to dissociation of the PP1-I-2 complex and activation of PP1.[46] In addition, PNUTS and PP1 promote DNA double-strand breaks by fine tuning the phosphorylation of DNA-dependent protein kinase catalytic subunit, DNA-PKcs.[47]

Among the 200 PIPs, we identified NIPP1 as a regulator of PP1γ of H3-pThr^{11}. NIPP1 was originally identified as a potent and specific inhibitor of PP1[8] through its interaction mainly at a defined RVxF motif.[12,13] NIPP1 has been implicated in pre-mRNA splicing, which is required for spliceosome formation,[7] by interacting with the splicing factors CDC5L and SAP155.[48,49] Furthermore, NIPP1 acts as a transcriptional repressor via interactions with the PRC2 (polycomb repressive complex 2) proteins Ezh2 and EED.[50,51] The forkhead-associated (FHA) domain has been shown to play an important role in numerous biological processes, such as DNA damage response and cell proliferation. NIPP1 contains an FHA domain, through which it interacts with CDC5L.[48] Further study will be needed to prove the role of this domain in DNA damage-induced transcriptional regulation.

Changes in PP1–NIPP1 interactions have important physiological consequences. For example, in response to cellular stress, such as heat shock, PP1 dissociates from NIPP1, which triggers PP1 activation. Activated PP1 then dephosphorylates SRp38 and regulates pre-mRNA splicing.[52] In addition, during hypoxia, basal intracellular cAMP is reduced, leading to a reduction in both PKA kinase activity and subsequent phosphorylation of NIPP1. This results in increased binding of NIPP1 to PP1, and the inhibition of PP1 activity.[53]

We analyzed publicly available RNA sequencing data performed in NIPP1-depleted testes.[19] Consistent with the observed phenotype in the NIPP1-KO testis, the E2F and MYC target genes were found to be downregulated. The E2F transcription factors consist of 9 members and are subdivided into 2 groups based on their functional characteristics: activators (E2F1-3a) or repressors (E2F3b-8) of transcription. Our data suggested that NIPP1 contributes to cell cycle progression by its ability to activate the transcription of E2F1 target genes, most likely via the PP1 inhibitory function.

Importantly, NIPP1 knockout mice are embryonically lethal at the onset of gastrulation, and NIPP1 knockdown cells also show

proliferation defects.[31,54] These results indicated that NIPP1 is essential for embryonic development and cell proliferation. In addition, the depletion of NIPP1 in the testis has been previously found to result in the reduced proliferation and increased apoptosis of spermatogonia and early meiotic spermatocytes.[19] Our model is consistent with reports showing that NIPP1 depletion results in defective G1/S progression.[19] Using CRISPR/Cas9-mediated NIPP1-depleted cells, we found that NIPP1 contributed to the induction of cell cycle progression through the expression of E2F1 target genes.

Consistent with these results, we also found that NIPP1 was upregulated in COAD, ESCA, LUAD, LUSC, and STAD, suggesting that the deregulated expression of NIPP1 may function as a potential oncogene. Taken together, our findings shed light on the role of NIPP1 in activating the transcription of E2F1 target genes, and indicate that NIPP1 has potential as a drug target for cancer therapy.

In summary, our results elucidated detailed mechanisms for the regulation of H3-Thr[11] phosphorylation by PP1γ. The interaction of PP1 and NIPP1 is responsible for the control of multiple pathways, such as heat shock and hypoxia. This work provides a basis for future studies to determine whether transcription following heat shock or hypoxia is also regulated by H3-Thr[11] phosphorylation.

ACKNOWLEDGMENTS

We thank Ms. N. Kawasaki for technical assistance, Dr. K. Nakayama and Dr. A. Matsumoto for providing materials and critical comments, and Dr. H. Miyoshi and Dr. N. Tanuma for providing materials. This work was supported by the Research Fellowships of the Japanese Society for the Promotion of Science (Grant Number 18H02681) (MS) and a grant from MSD Life Science Foundation, Public Interest Incorporated Foundation (MS).

CONFLICT OF INTEREST

The authors declare that they have no competing interests.

ORCID

Shunsuke Hanaki https://orcid.org/0000-0002-7803-0547
Makoto Habara https://orcid.org/0000-0001-6418-1291
Takahiro Masaki https://orcid.org/0000-0002-2948-0277
Keisuke Maeda https://orcid.org/0000-0002-5278-4500
Yuki Sato https://orcid.org/0000-0002-4137-6042
Makoto Nakanishi https://orcid.org/0000-0002-6707-3584
Midori Shimada https://orcid.org/0000-0002-2718-8600

REFERENCES

1. Shimada M, Niida H, Zineldeen DH, et al. Chk1 is a histone H3 threonine 11 kinase that regulates DNA damage-induced transcriptional repression. *Cell*. 2008;132:221-232.
2. Shimada M, Haruta M, Niida H, Sawamoto K, Nakanishi M. Protein phosphatase 1gamma is responsible for dephosphorylation of histone H3 at Thr 11 after DNA damage. *EMBO Rep*. 2010;11:883-889.
3. Shimada M, Nakanishi M. Response to DNA damage: why do we need to focus on protein phosphatases? *Front Oncol*. 2013;3:8.
4. Lemonnier T, Dupre A, Jessus C. The G2-to-M transition from a phosphatase perspective: a new vision of the meiotic division. *Cell Div*. 2020;15:9.
5. Cohen PT. Protein phosphatase 1–targeted in many directions. *J Cell Sci*. 2002;115:241-256.
6. Aggen JB, Nairn AC, Chamberlin R. Regulation of protein phosphatase-1. *Chem Biol*. 2000;7:R13-23.
7. Beullens M, Bollen M. The protein phosphatase-1 regulator NIPP1 is also a splicing factor involved in a late step of spliceosome assembly. *J Biol Chem*. 2002;277:19855-19860.
8. Beullens M, Van Eynde A, Stalmans W, Bollen M. The isolation of novel inhibitory polypeptides of protein phosphatase 1 from bovine thymus nuclei. *J Biol Chem*. 1992;267:16538-16544.
9. Beullens M, Van Eynde A, Vulsteke V, et al. Molecular determinants of nuclear protein phosphatase-1 regulation by NIPP-1. *J Biol Chem*. 1999;274:14053-14061.
10. Tanuma N, Kim SE, Beullens M, et al. Nuclear inhibitor of protein phosphatase-1 (NIPP1) directs protein phosphatase-1 (PP1) to dephosphorylate the U2 small nuclear ribonucleoprotein particle (snRNP) component, spliceosome-associated protein 155 (Sap155). *J Biol Chem*. 2008;283:35805-35814.
11. Beullens M, Van Eynde A, Bollen M, Stalmans W. Inactivation of nuclear inhibitory polypeptides of protein phosphatase-1 (NIPP-1) by protein kinase A. *J Biol Chem*. 1993;268:13172-13177.
12. Beullens M, Vulsteke V, Van Eynde A, Jagiello I, Stalmans W, Bollen M. The C-terminus of NIPP1 (nuclear inhibitor of protein phosphatase-1) contains a novel binding site for protein phosphatase-1 that is controlled by tyrosine phosphorylation and RNA binding. *Biochem J*. 2000;352(Pt 3):651-658.
13. Van Eynde A, Beullens M, Stalmans W, Bollen M. Full activation of a nuclear species of protein phosphatase-1 by phosphorylation with protein kinase A and casein kinase-2. *Biochem J*. 1994;297(Pt 3):447-449.
14. Vulsteke V, Beullens M, Waelkens E, Stalmans W, Bollen M. Properties and phosphorylation sites of baculovirus-expressed nuclear inhibitor of protein phosphatase-1 (NIPP-1). *J Biol Chem*. 1997;272:32972-32978.
15. da Huang W, Sherman BT, Lempicki RA. Bioinformatics enrichment tools: paths toward the comprehensive functional analysis of large gene lists. *Nucleic Acids Res*. 2009;37:1-13.
16. da Huang W, Sherman BT, Lempicki RA. Systematic and integrative analysis of large gene lists using DAVID bioinformatics resources. *Nat Protoc*. 2009;4:44-57.
17. Chen H, Boutros PC. VennDiagram: a package for the generation of highly-customizable Venn and Euler diagrams in R. *BMC Bioinformatics*. 2011;12:35.
18. Goshima T, Habara M, Maeda K, Hanaki S, Kato Y, Shimada M. Calcineurin regulates cyclin D1 stability through dephosphorylation at T286. *Sci Rep*. 2019;9:12779.
19. Ferreira M, Boens S, Winkler C, et al. The protein phosphatase 1 regulator NIPP1 is essential for mammalian spermatogenesis. *Sci Rep*. 2017;7:13364.
20. Martin M. Cutadapt Removes Adapter Sequences From High-Throughput Sequencing Reads. *EMBnetjournal*. 2011;17(1):10.
21. Schmieder R, Edwards R. Quality control and preprocessing of metagenomic datasets. *Bioinformatics*. 2011;27:863-864.
22. Steward CA, Humphray S, Plumb B, et al. Genome-wide end-sequenced BAC resources for the NOD/MrkTac and NOD/ShiLtJ mouse genomes. *Genomics*. 2010;95:105-110.
23. Church DM, Goodstadt L, Hillier LW, et al. Lineage-specific biology revealed by a finished genome assembly of the mouse. *PLoS Biol*. 2009;7:e1000112.
24. Church DM, Schneider VA, Graves T, et al. Modernizing reference genome assemblies. *PLoS Biol*. 2011;9:e1001091.

25. Bayona-Bafaluy MP, Acin-Perez R, Mullikin JC, et al. Revisiting the mouse mitochondrial DNA sequence. *Nucleic Acids Res*. 2003;31:5349-5355.
26. Patro R, Duggal G, Love MI, Irizarry RA, Kingsford C. Salmon provides fast and bias-aware quantification of transcript expression. *Nat Methods*. 2017;14:417-419.
27. Soneson C, Love MI, Robinson MD. Differential analyses for RNA-seq: transcript-level estimates improve gene-level inferences. *F1000Res*. 2015;4:1521.
28. Subramanian A, Tamayo P, Mootha VK, et al. Gene set enrichment analysis: a knowledge-based approach for interpreting genome-wide expression profiles. *Proc Natl Acad Sci U S A*. 2005;102:15545-15550.
29. Liberzon A, Birger C, Thorvaldsdottir H, Ghandi M, Mesirov JP, Tamayo P. The Molecular Signatures Database (MSigDB) hallmark gene set collection. *Cell Syst*. 2015;1:417-425.
30. Sawicka A, Hartl D, Goiser M, et al. H3S28 phosphorylation is a hallmark of the transcriptional response to cellular stress. *Genome Res*. 2014;24:1808-1820.
31. Nuytten M, Beke L, Van Eynde A, et al. The transcriptional repressor NIPP1 is an essential player in EZH2-mediated gene silencing. *Oncogene*. 2008;27:1449-1460.
32. Bracken AP, Ciro M, Cocito A, Helin K. E2F target genes: unraveling the biology. *Trends Biochem Sci*. 2004;29:409-417.
33. Oki S, Ohta T, Shioi G, et al. ChIP-Atlas: a data-mining suite powered by full integration of public ChIP-seq data. *EMBO Rep*. 2018;19:e46255.
34. Heroes E, Lesage B, Gornemann J, Beullens M, Van Meervelt L, Bollen M. The PP1 binding code: a molecular-lego strategy that governs specificity. *FEBS J*. 2013;280:584-595.
35. Winkler C, Rouget R, Wu D, Beullens M, Van Eynde A, Bollen M. Overexpression of PP1-NIPP1 limits the capacity of cells to repair DNA double-strand breaks. *J Cell Sci*. 2018;131:jcs214932.
36. Landsverk HB, Mora-Bermudez F, Landsverk OJ, et al. The protein phosphatase 1 regulator PNUTS is a new component of the DNA damage response. *EMBO Rep*. 2010;11:868-875.
37. De Leon G, Cavino M, D'Angelo M, Krucher NA. PNUTS knockdown potentiates the apoptotic effect of Roscovitine in breast and colon cancer cells. *Int J Oncol*. 2010;36:1269-1275.
38. Wang F, Wang L, Fisher LA, Li C, Wang W, Peng A. Phosphatase 1 nuclear targeting subunit (PNUTS) regulates aurora kinases and mitotic progression. *Mol Cancer Res*. 2019;17:10-19.
39. Adams JA, McGlone ML, Gibson R, Taylor SS. Phosphorylation modulates catalytic function and regulation in the cAMP-dependent protein kinase. *Biochemistry*. 1995;34:2447-2454.
40. Jarrett SG, Wolf Horrell EM, Christian PA, et al. PKA-mediated phosphorylation of ATR promotes recruitment of XPA to UV-induced DNA damage. *Mol Cell*. 2014;54:999-1011.
41. Wells J, Boyd KE, Fry CJ, Bartley SM, Farnham PJ. Target gene specificity of E2F and pocket protein family members in living cells. *Mol Cell Biol*. 2000;20:5797-5807.
42. Zhang HS, Gavin M, Dahiya A, et al. Exit from G1 and S phase of the cell cycle is regulated by repressor complexes containing HDAC-Rb-hSWI/SNF and Rb-hSWI/SNF. *Cell*. 2000;101:79-89.
43. Rayman JB, Takahashi Y, Indjeian VB, et al. E2F mediates cell cycle-dependent transcriptional repression in vivo by recruitment of an HDAC1/mSin3B corepressor complex. *Genes Dev*. 2002;16:933-947.
44. Blais A, Dynlacht BD. E2F-associated chromatin modifiers and cell cycle control. *Curr Opin Cell Biol*. 2007;19:658-662.
45. Qian J, Lesage B, Beullens M, Van Eynde A, Bollen M. PP1/Repoman dephosphorylates mitotic histone H3 at T3 and regulates chromosomal aurora B targeting. *Curr Biol*. 2011;21:766-773.
46. Tang X, Hui ZG, Cui XL, Garg R, Kastan MB, Xu B. A novel ATM-dependent pathway regulates protein phosphatase 1 in response to DNA damage. *Mol Cell Biol*. 2008;28:2559-2566.
47. Zhu S, Fisher LA, Bessho T, Peng A. Protein phosphatase 1 and phosphatase 1 nuclear targeting subunit-dependent regulation of DNA-dependent protein kinase and non-homologous end joining. *Nucleic Acids Res*. 2017;45:10583-10594.
48. Boudrez A, Beullens M, Groenen P, et al. NIPP1-mediated interaction of protein phosphatase-1 with CDC5L, a regulator of pre-mRNA splicing and mitotic entry. *J Biol Chem*. 2000;275:25411-25417.
49. Deckert J, Hartmuth K, Boehringer D, et al. Protein composition and electron microscopy structure of affinity-purified human spliceosomal B complexes isolated under physiological conditions. *Mol Cell Biol*. 2006;26:5528-5543.
50. Jin Q, van Eynde A, Beullens M, et al. The protein phosphatase-1 (PP1) regulator, nuclear inhibitor of PP1 (NIPP1), interacts with the polycomb group protein, embryonic ectoderm development (EED), and functions as a transcriptional repressor. *J Biol Chem*. 2003;278:30677-30685.
51. Roy N, Van Eynde A, Beke L, Nuytten M, Bollen M. The transcriptional repression by NIPP1 is mediated by Polycomb group proteins. *Biochim Biophys Acta*. 2007;1769:541-545.
52. Shi Y, Manley JL. A complex signaling pathway regulates SRp38 phosphorylation and pre-mRNA splicing in response to heat shock. *Mol Cell*. 2007;28:79-90.
53. Comerford KM, Leonard MO, Cummins EP, et al. Regulation of protein phosphatase 1gamma activity in hypoxia through increased interaction with NIPP1: implications for cellular metabolism. *J Cell Physiol*. 2006;209:211-218.
54. Van Eynde A, Nuytten M, Dewerchin M, et al. The nuclear scaffold protein NIPP1 is essential for early embryonic development and cell proliferation. *Mol Cell Biol*. 2004;24:5863-5874.

SUPPORTING INFORMATION

Additional supporting information may be found online in the Supporting Information section.

How to cite this article: Hanaki S, Habara M, Masaki T, et al. PP1 regulatory subunit NIPP1 regulates transcription of E2F1 target genes following DNA damage. *Cancer Sci*. 2021;112:2739–2752. https://doi.org/10.1111/cas.14924